NASA-CR-193028

Six Degree of Freedom
Active Vibration Damping for Space Application

Contract Number NAS7-1198

IN-39-CR
161911
p, 31

Quarterly Progress Report

Third Quarter

January 1, 1993 through March 31, 1993

Submitted to:
National Aeronautics and Space Administration
Jet Propulsion Laboratory
4800 Oak Grove Drive
Pasadena, CA 91109

Submitted By:

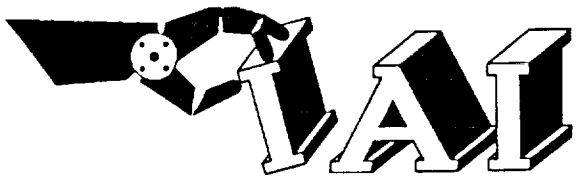

Intelligent Automation, Incorporated
1370 Piccard Drive, Suite 210
Rockville, Maryland 20850
301-990-2407

Expenditures
Contract No. NAS7-1198

Third Quarter: 1/1/93 - 3/31/93

planned expenditures

actual expenditures

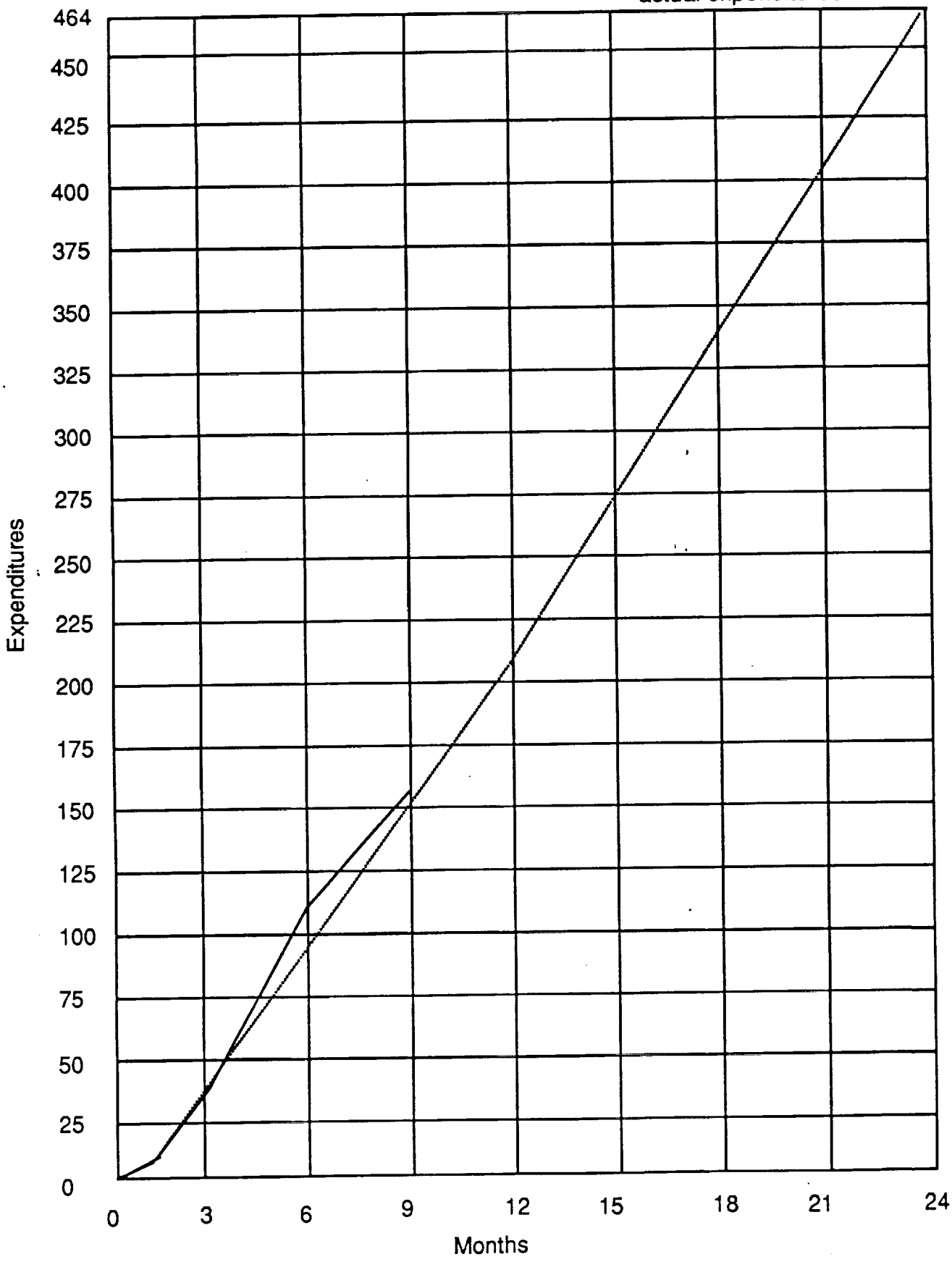

Performance and Cost Report

DIN A001

Contract NAS7-1198

THIRD QUARTER

January 1, 1993 - March 31, 1993

Supplied by Leonard S. Haynes, Ph.D.
Principal Investigator

Intelligent Automation, Inc.
1370 Piccard Drive, Suite 210
Rockville, MD 20850

Salaries			
	Dr. Leonard S. Haynes	71 hours	$3,479.00
	Dr. Zheng Geng	282 hours	$8,648.94
	Dr. Jacqueline Haynes	0 hours	$0.00
	George Pan	152 hours	$2,995.92
	Dr. Joe Teter	110 hours	$1,176.00
	Total Direct Labor		$16,299.86
Overhead on Direct Labor			$18,092.84
Travel			$1,370.74
Subcontract			$1,390.00
Materials/Supplies			$1,853.46
Consultants			$885.00
Telephone, Postage			$103.30
Total Expenditures, Second Quarter			**$39,995.20**
Total Contract Expenses to Date			**$154,211.69**

Active Vibration Control for Large Space Structure

Quarterly Progress Report # 3
(UNCLASSIFIED)

Contract # NAS7 -1198
Sponsored by National Aeronautics and Space Administration

Progress For the Period : January 31, 1993 to April 30, 1993
Submitted: May 2, 1993

Intelligent Automation, Inc.
1370 Piccard Drive, Rockville, MD 20850
(301) 990 - 2407

Milestones

Milestone No.		Month	% completed
1.1	Alternative actuator design completed	4	90
1.2	Alternative actuator fabricated and procured	6	70
2.1	Sensors and design mounting hardware selected and fabricated	4	60
2.2	Flex joints, lower and upper plates designed and fabricated	4	70
2.3	All platform hardware fabricated and assembled	6	0
2.4	Signal conditioning electronics designed and fabricated	6	50
3.1	Re-host the adaptive filter algorithms from Phase I	6	90
3.2	Select and procure host computer and data I/O hardware	6	75
3.3	Adaptive filter algorithms re-coded on new hardware	9	60
4.1	Characterize the cryogenic cooler of JPL	9	20
4.2	Vibration testbed	9	0
4.3	Adaptive filter algorithm optimized	9	30
5.	Evaluate the effect of load on the system	14	20
6.	Evaluate the frequency response of the system	14	40

7.	Evaluate the impact of vibration magnitude on the performance	15	20
8.1	Parameters which can be measured by internally generated vibrations and by internally measured responses identified.	16	0
8.2	Software parameterized so that the control algorithms exploit the measured parameters for self-test and re-calibration.	20	0
9.1	Access to large truss testbed obtained, or an IAI testbed constructed.	14	0
9.2	Tests which quantify the ability of our system to isolate vibrating components from a space structure designed.	16	0
10.1	Required system characteristics in terms of power consumption, voltages, control protocols, self test requirements, identified.	18	0
10.2	System design optimized for the above characteristics.	20	0
11.1	Cubic section of the truss of the CSI Phase B Testbed (or our own testbed truss) implemented using six active legs configured as a cubic Stewart Platform.	16	0
11.2	Use of the cubic configuration as a component of the NASA JPL CSI Phase B Testbed fully evaluated.	24	0
12	Feasibility for space qualification of a Phase 3 system evaluated.	24	0
13.1	Potential commercial applications identified.	12	20
13.2	Demonstrate applicability of the vibration control hardware and software to the identified commercial problems.	24	20
13.3	Potential supporters of Phase 3 development identified.	24	0

Informal Technical Information

1. Actuator Testing

The test results for our current actuators in the low frequency range have been reported in prior reports. We have recently conducted several new tests to our current Terfenol actuators to study their frequency response, especially in the higher frequency range. Using a Hewlett Packard combined impedance/spectrum analyzer, we measured the acceleration response of the current actuators. We also monitored the impedance of the actuator during the test. Since the Terfenol material is a nonlinear material and it may exhibit different behavior at different levels of control current, we tested the transfer function of the actuator at 15 volt, 30 volt, and 60 volt input signal levels. At the lower excitation input level, the transfer functions looked very similar. Some of results are shown in Figure 1.1 There is no significant structural mode at the frequency range below 3000 Hz.

The prototype of our new design of actuator has also been tested. Figure 1.2 shows the displacement response of the prototype actuator at different input current levels, as well as their power spectrums. As shown in the figures, the response is fairly linear at lower current drive levels. The responses degrade with larger amplitude inputs. The test input signal is a 25 Hz sinusoidal. The displacement measurement device used was an LVDT. Since the LVDT device is essentially a DC measurement device, it own resonant mode is about 10 Hz, and may effect our results. We are investigating this issue now. We plan to use a capacitance probe to obtain more accurate measurements, and the National Institute of Standards and Technology has loaned us a capacitance probe for this purpose. The results will be reported in the next progress period.

2. Mechanical Amplifier Design

We have finalized our mechanical amplifier design, as shown in Figure 2.1. The simulation data for the amplification ratio of an ideal design model is shown in Figure 2.2, where the ratio Rm is approximately 4.5. The actual amplification ration for our amplifier is expected to be 2.5 to 3.0. We have contracted with ComSat to fabricate the hardware for the amplifier.

Some of design issues of the flexure based mechanical amplifier are discussed as follows:

Advantages of flexures :

(1) There is no backlash which is usually a problem of using conventional joints for precision devices.

(2) They are wear free because there are no sliding pairs. The only likely wear mechanisms will be fretting and corrosion at fabricated interfaces where changing stresses are applied.

(3) They can be manufactured from a single piece of material to provide a monolithic structure;

(4) Displacements are smooth and continuous at all levels.

Disadvantages:

(1) There will be hysteresis due to dislocation movement in most materials. Its magnitude depends upon the stress level, temperature and the grain structure and atomic bonding in the material.

(2) They can only facilitate small displacement for a given size and stiffness.

(3) They cannot tolerate large loads. Unless precautions are taken, accidental overloads can lead to fatigue, work hardening and eventually to catastrophic failure.

Stiffness of Flexures

A flexure joint can be modelled as a simple cantilever beam:

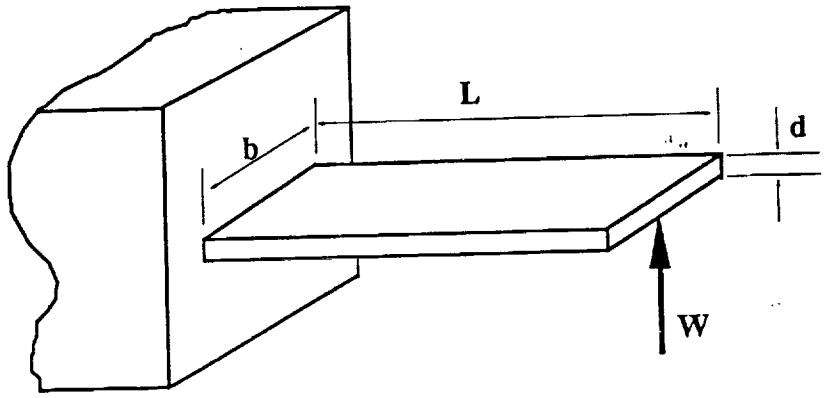

The stiffness of the flexure under transverse load W can be expressed as:

$$\lambda = \frac{12\,E\,I}{L^3} = \frac{E\,b\,d^3}{L^3}$$

where: E is the Young's Modulus of the material;
I is the second moment of the cross-sectional area. For rectangular cross-section,

$$I = \frac{b\,d^3}{12}$$

Hinge Bending Angle Estimation

Based on the beam theory, the hinge bending angle can be approximated as

$$\theta = \frac{W\,L^3}{2\,E\,I}$$

where θ is the bending angle at the tip of the hinge in radians, W is transversal load. Rearranging the above equation, we have :

$$W = \frac{2 E I \theta}{L^3} = \frac{E b d^3 \theta}{6 L^3}$$

Numerical example:

In the joint we designed
E = 136500 (=210000*0.65) N/mm^2 (for Beryllium copper)
b = 0.5 in = 12.7 mm
d = 0.01 in = 0.254 mm
L = 0.1 in = 2.54 mm
θ = 1 degree = 0.01745 rad

$W = 136500 * 12.7 * 0.254^3 * 0.01745 / (6 * 2.54^3) = 5.04$ N

Maximum Deflection Range

The deflection range of a flexure stage will be governed either by its stiffness, through a maximum force that can be applied to it, or by its elastic properties. Using simple beam theory, this limit will occur when a maximum allowable tensile stress is reached at the section of maximum bending moment. The maximum permissible displacement is

$$q_{max} = \frac{\sigma_{max} L^2}{3 E d}$$

Referring to the above equations, increasing the thickness of the blade d will rapidly increase overall stiffness with little weight penalty. However the deflection that can be obtained without exceeding a specified maximum stress decreases linearly with the thickness. The width of the blade linearly effects both stiffness and weight without influencing maximum deflection.

Euler Buckling Load

The buckling should also be considered in the flexure design.

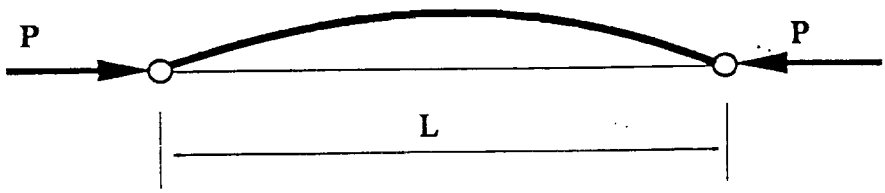

The critical load or buckling load is derived as:

$$P_E = \pi^2 \frac{E I}{L^2} = \frac{\pi^2 E d b^3}{12 L^2}$$

Numerical example:

In the joint we designed
$E = 136500$ (=210000*0.65) N/mm^2 (for Beryllium copper)
$b = 0.5$ in $= 12.7$ mm
$d = 0.01$ in $= 0.254$ mm
$L = 0.1$ in $= 2.54$ mm

$$P_E = (\pi^2 /12) (136500 * 12.7 * 0.254^3 / 2.54^2) = 3621.5 \text{ N}$$

Material Selection

A set of functional requirement can be established to guide the selection of materials. The flexure joint must have a good repeatability, implying a material with a good dimensional stability and low hysteresis loss. The material must be able to sustain considerable stress to allow a large degree of flexure. High resonance will be desirable in order to reduce the control-structure interaction, so low mass and high mechanism stiffness are wanted.

Beryllium copper has very good yield strength therefore allows greater deflection of the flexures. We are fabricating the prototype mechanicl amplifier out of berillium copper, however in a final design titanium would be a better choice.

3. Neural Network Control System Development and Experimental Evaluation

Vibration control of structures can be achieved by passive or active means. A typical passive damping technique, which is effective in damping out higher frequency vibration, exploits viscoelastic materials. Better performance at lower frequencies with less weight can be achieved using active controls. However, design of an active vibration control system is a challenging task because of the large number of structural modes involved in the bandwidth of interest, and the large amount of uncertainty involved. In our application, the problem is exacerbated by the fact that the dynamic behavior of these systems will hardly be known precisely during design, and identification of the system model will provide only limited information because of uncertainties such as dynamic perturbations, transient thermal states, parameter drift, etc. This raises concern as to robustness and stability.

There have been a number of active vibration isolation approaches proposed in recent years. The control design of most of these approaches relies on model information to predict the structure's dynamic response. In reality, a perfect model of a lightly damped space structure has an infinite number of lightly damped modes. Consequently, higher order modes are truncated from the model in order to perform effective control design. The model-based control design, such as LQG optimal control, pole-zero cancellation, etc., will work well as long as the modes included in the model are accurately compensated, and the unmodelled modes are sufficiently damped. In the case where there are closely spaced higher order unmodelled modes, the performance of such a control design will severely deteriorate, even resulting in instability.

3.1 Neural network structure and backpropagation algorithm

A multilayer feedforward neural network model consists of an input layer, one or more hidden layers, and an output layer of neurons with full connections between neurons in these layers. Assume that a single neuron has a structure shown in figure 3.1, where $X_k = [\, x_0, x_{1k}, x_{2k}, \ldots, x_{nk} \,]$ is input vector, and the subscript k denote the adaptation index. $W_k = [\, w_{0k}, w_{1k}, w_{2k}, \ldots, w_{nk} \,]$ is the weight vector which is to be adjusted during the adaptation to minimize the error.

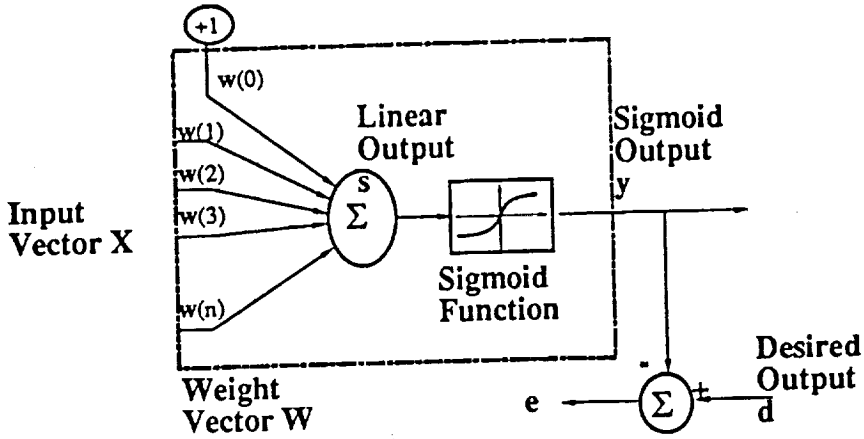

Figure 3.1 Structure of a Single Neuron

The output of the neuron is calculated by:

$$y_k = \mathrm{sgm}(s_k) = \mathrm{sgm}(\, W_k^T X_k) \tag{3.1}$$

where sgm represents a sigmoid mapping function of the linear output signal s.

The learning process of the network begins by presenting an input vector X to the network, sweeping forward through the system to generate an output response vector Y, and computing the errors at each output. The objective of the adaptation (learning) algorithm is to minimize the mean square of the sigmoid error defined as:

$$e_k = d_k - y_k = d_k - \mathrm{sgm}(s_k) \tag{3.2}$$

The instantaneous gradient estimate obtained at the kth adaptation cycle is given by:

$$\nabla_{w_k} = \frac{\partial\, (e_k)^2}{\partial\, w_k} = 2\, e_k \frac{\partial\, e_k}{\partial\, w_k} = 2\, e_k \left[- \frac{\partial\, \mathrm{sgm}(s_k)}{\partial\, w_k} \right]$$

$$= - 2\, e_k\, \mathrm{sgm}'(s_k) \frac{\partial\, s_k}{\partial\, w_k} = - 2\, e_k\, \mathrm{sgm}'(s_k)\, X_k \tag{3.3}$$

therefore for a general sigmoid function, the adaptation law is

$$W_{k+1} = W_k + \mu\, (- \nabla_{w_k})$$

$$= W_k + 2\, \mu\, e_k\, \mathrm{sgm}'(s_k)\, X_k \tag{3.4}$$

where μ is a positive-value learning rate constant.

For the purpose of error correction, the output error at the output layer neuron should be back-propagated into hidden layers based on chain rules. From a single neuron point of view, the error back-propagation algorithm is derived as:

$$\nabla_{X_k} = \frac{\partial (e_k)^2}{\partial X_k} = 2 e_k \frac{\partial e_k}{\partial X_k} = 2 e_k [- \frac{\partial sgm(s_k)}{\partial X_k}]$$
$$= - 2 e_k sgm'(s_k) \frac{\partial s_k}{\partial X_k} = - 2 e_k sgm'(s_k) W_k \qquad (3.5)$$

In the case where the sigmoid function is the hyperbolic tangent function tanh(.) :

$$y_k = sgm(s_k) = \tanh(s_k) = (\frac{1 - e^{-2 s_k}}{1 + e^{-2 s_k}}) \qquad (3.6)$$

we then have

$$sgm'(s_k) = \frac{\partial (\tanh(s_k))}{\partial s_k} = 1 - (\tanh(s_k))^2 = 1 - (sgm(s_k))^2 = 1 - y_k^2 \qquad (3.7)$$

The adaptation law becomes:

$$W_{k+1} = W_k + 2 \mu \ e_k (1 - y_k^2) X_k \qquad (3.8)$$

3.2 Control System Structure

(1) Direct learning control

In direct control, the parameters of the controller are directly adjusted to reduce the output error.

(2) Indirect learning control

In the indirect control, the dynamic behavior of the plant is first identified by a neural network model and then the adjustment of the controller is performed based on the output error and the system model.

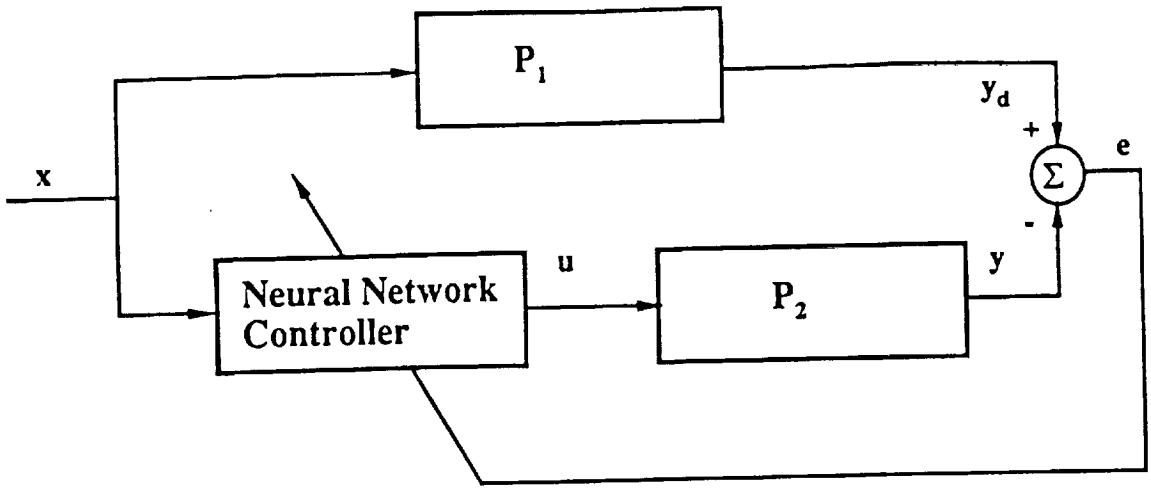

Figure 3.2 A Neural Controller for Active Vibration Control

Figure 3.2 depicts a basic scenario of single channel active vibration control, where P_1 denotes the transfer function (TF) of the primary channel of the system, and P_2 denotes the TF of the secondary channel of the system. The vibration source **x** , which can be measured by input sensors, excites the primary channel to generate uncontrollable undesirable vibration disturbance y_d at the output sensor location. The output vibration disturbance **e** is picked up by output sensor(s) and sent to an adaptive filter with the input sensor signal for active control signal generation. As shown in the figure, the neural controller output **u** is fed into an actuator(secondary channel) P_2 which produces proper anti-vibration y to cancel the vibration at output sensor location.

For the sake of simplicity, assume that the architecture of the neural network controller is a single neuron with N inputs. At the k^{th} sampling instance, the input vector consists of the N taps of history data of the reference signal x: [x(k), x(k-1),...,x(k-N+1)].
Therefore

$$u(j) = sgm[\sum_{i=0}^{N-1} w_i\, x(j-i)] \tag{3.9}$$

Without loss generality, let the dynamics of the secondary channel P_2 be described as:

$$y(k) = P_2[\, u(k-1), u(k-2), \ldots, u(k-M)\,] \tag{3.10}$$

or

$$y(k) = P_2[\, sgm[\sum_{i=0}^{N-1} w_i\, x(k-i-1)\,], sgm[\sum_{i=0}^{N-1} w_i\, x(k-i-2)\,], \ldots, sgm[\sum_{i=0}^{N-1} w_i\, x(k-i-M)\,]\,]$$

The error signal is defined as:

$$e(k) = y_d(k) - y(k) \tag{3.11}$$

The gradient of the performance index $J = e^2(k)$ is calculated as:

$$\nabla_i = \frac{\partial\,(e(k))^2}{\partial\, w_i} = 2\, e(k) \frac{\partial\, e(k)}{\partial\, w_i} = -\,2\, e(k) \frac{\partial\, y(k)}{\partial\, w_i} \tag{3.12}$$

According to equation (3.10)

$$\frac{\partial\, y(k)}{\partial\, w_i} = \frac{\partial\, P_2}{\partial\, u(k-1)} \frac{\partial\, u(k-1)}{\partial\, w_i} + \frac{\partial\, P_2}{\partial\, u(k-2)} \frac{\partial\, u(k-2)}{\partial\, w_i} + \cdots + \frac{\partial\, P_2}{\partial\, u(k-M)} \frac{\partial\, u(k-M)}{\partial\, w_i}$$

or

$$\frac{\partial\, y(k)}{\partial\, w_i} = \sum_{j=1}^{M} \frac{\partial\, P_2}{\partial\, u(k-j)} \frac{\partial\, u(k-j)}{\partial\, w_i} \tag{3.13}$$

Based on the neuron model:

$$\frac{\partial\, u(k-j)}{\partial\, w_i} = \frac{\partial}{\partial\, w_i} sgm[\, \sum_{i=0}^{N-1} w_i\, x(k-j-i)\,] = (\,1 - u^2(k-j)\,)\, x(k-j-i) \tag{3.14}$$

substitute this result into equation (3.13)

$$\frac{\partial\, y(k)}{\partial\, w_i} = \sum_{j=1}^{M} \frac{\partial\, P_2}{\partial\, u(k-j)} (\,1 - u^2(k-j)\,)\, x(k-j-i) \tag{3.15}$$

The update law for the proposed neural controller is then:

$$w_i(k+1) = w_i(k) + 2\,\mu\, e(k) \sum_{j=1}^{M} \frac{\partial\, P_2}{\partial\, u(k-j)} (\,1 - u^2(k-j)\,)\, x(k-j-i) \tag{3.16}$$

In the case that the secondary channel can be modelled by another neuron, we have:

$$y(k) = sgm[\, \sum_{j=1}^{M} v_j\, u(k-j)\,] \tag{3.17}$$

The partial derivative becomes

$$\frac{\partial\, P_2}{\partial\, u(k-j)} = (\,1 - y^2(k)\,)\, v_j \tag{3.18}$$

the component of the gradient is:

$$\frac{\partial\, y(k)}{\partial\, w_i} = \sum_{j=1}^{M} (\,1 - y^2(k)\,)\, v_j\, (\,1 - u^2(k-j)\,)\, x(k-j-i)$$

or

$$\frac{\partial y(k)}{\partial w_i} = (1 - y^2(k)) \sum_{j=1}^{M} v_j (1 - u^2(k-j)) x(k-j-i) \tag{3.19}$$

The update law becomes:

$$w_i(k+1) = w_i(k) + 2 \mu e(k) (1 - y^2(k)) \sum_{j=1}^{M} v_j (1 - u^2(k-j)) x(k-j-i) \tag{3.20}$$

We have conducted experimental evaluation of the above neural control algorithm. One test result is shown in Figure 3.3, where about 20 dB attenuation was achieved. Application of this algorithm to multiple channel systems is under study and the result will be presented in the next progress report.

FRF15A/V

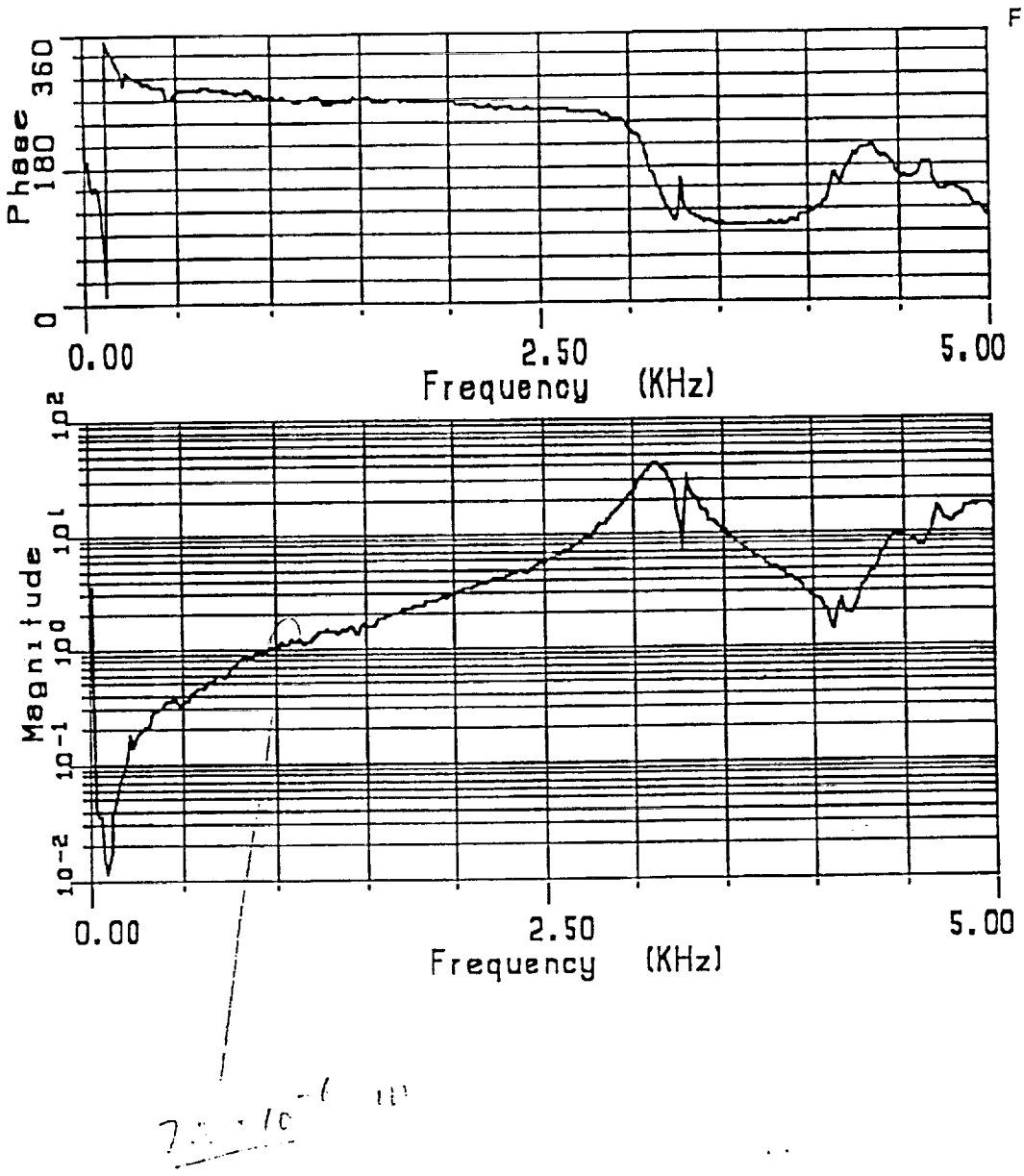

Figure 1.1 (a)

FRF30A/V

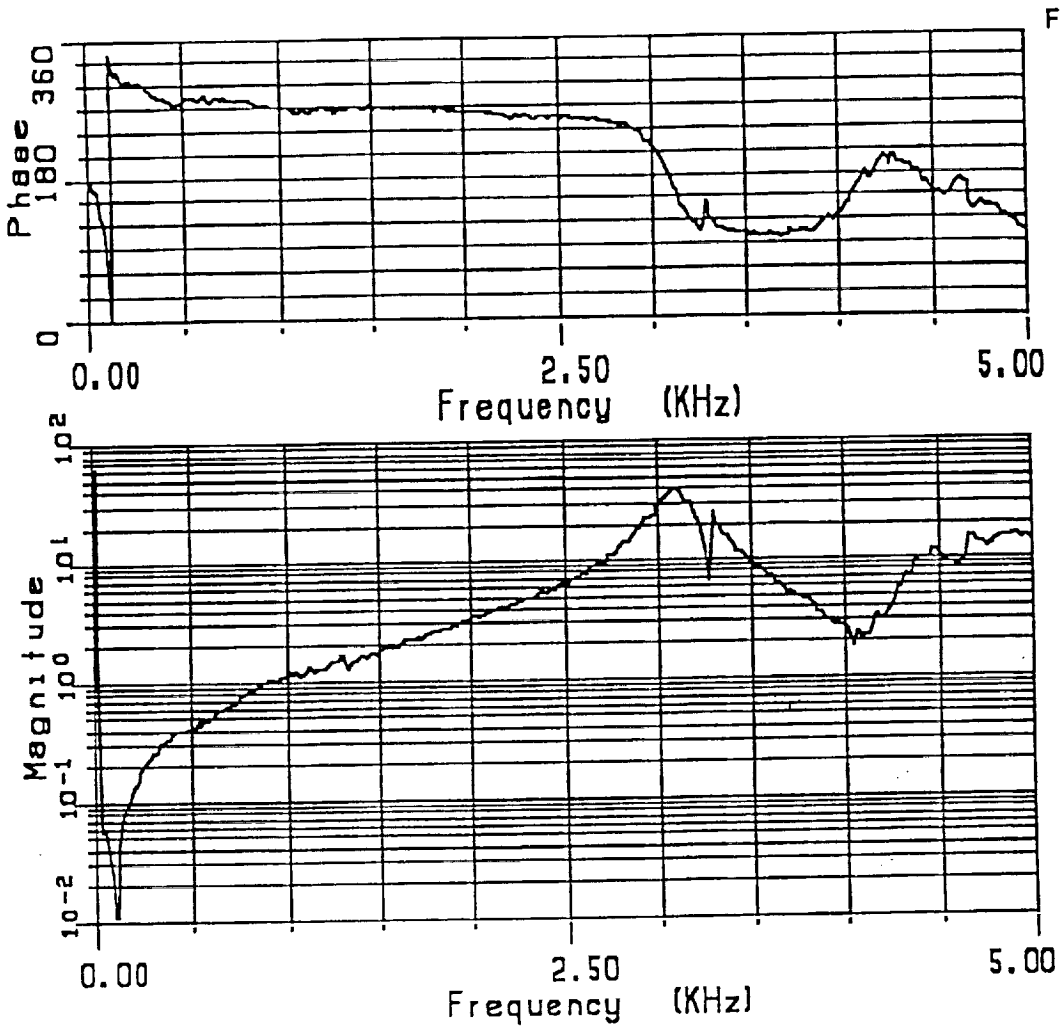

Figure 1.1 (b)

FRF60A/V

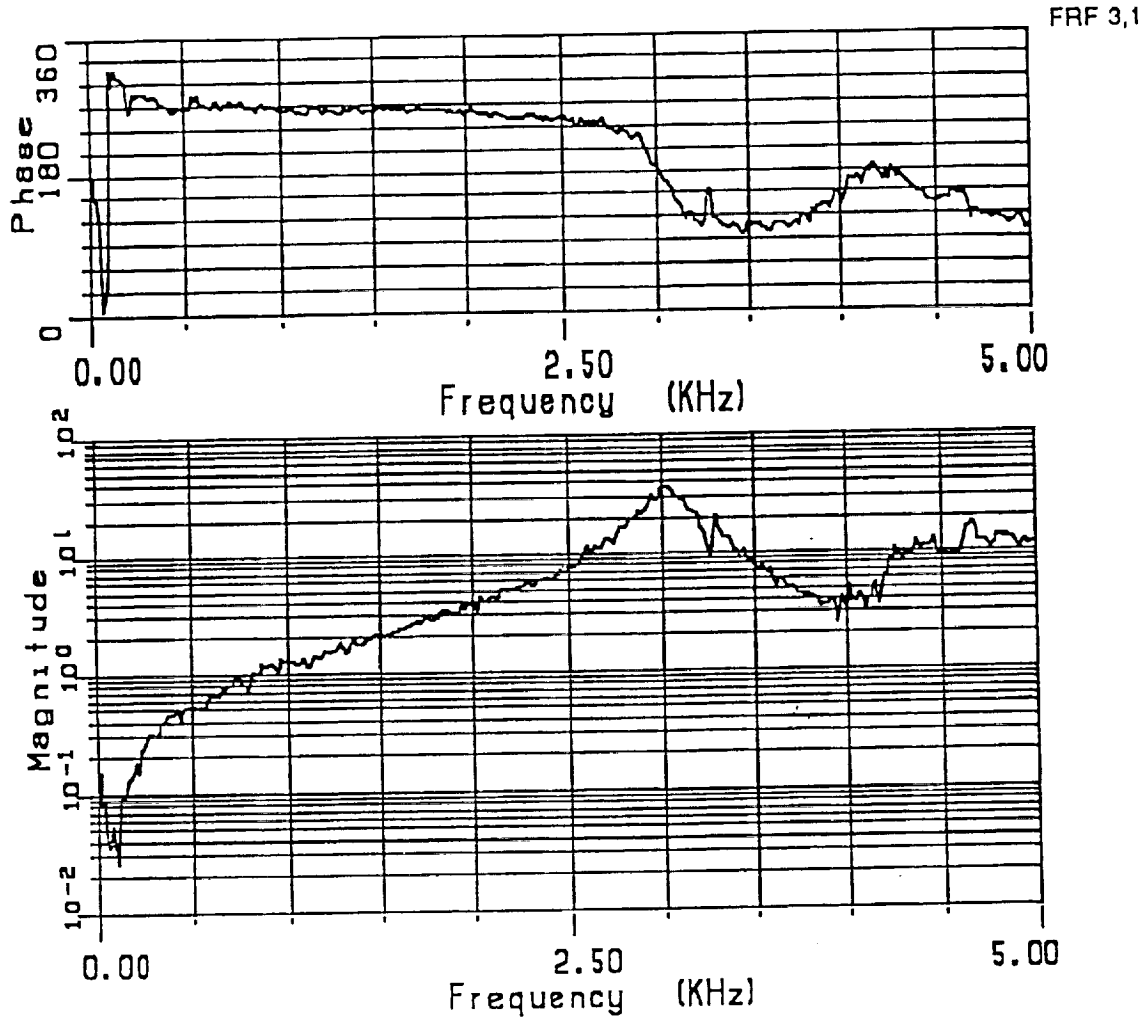

Figure 1.1 (c)

FRF15I/V

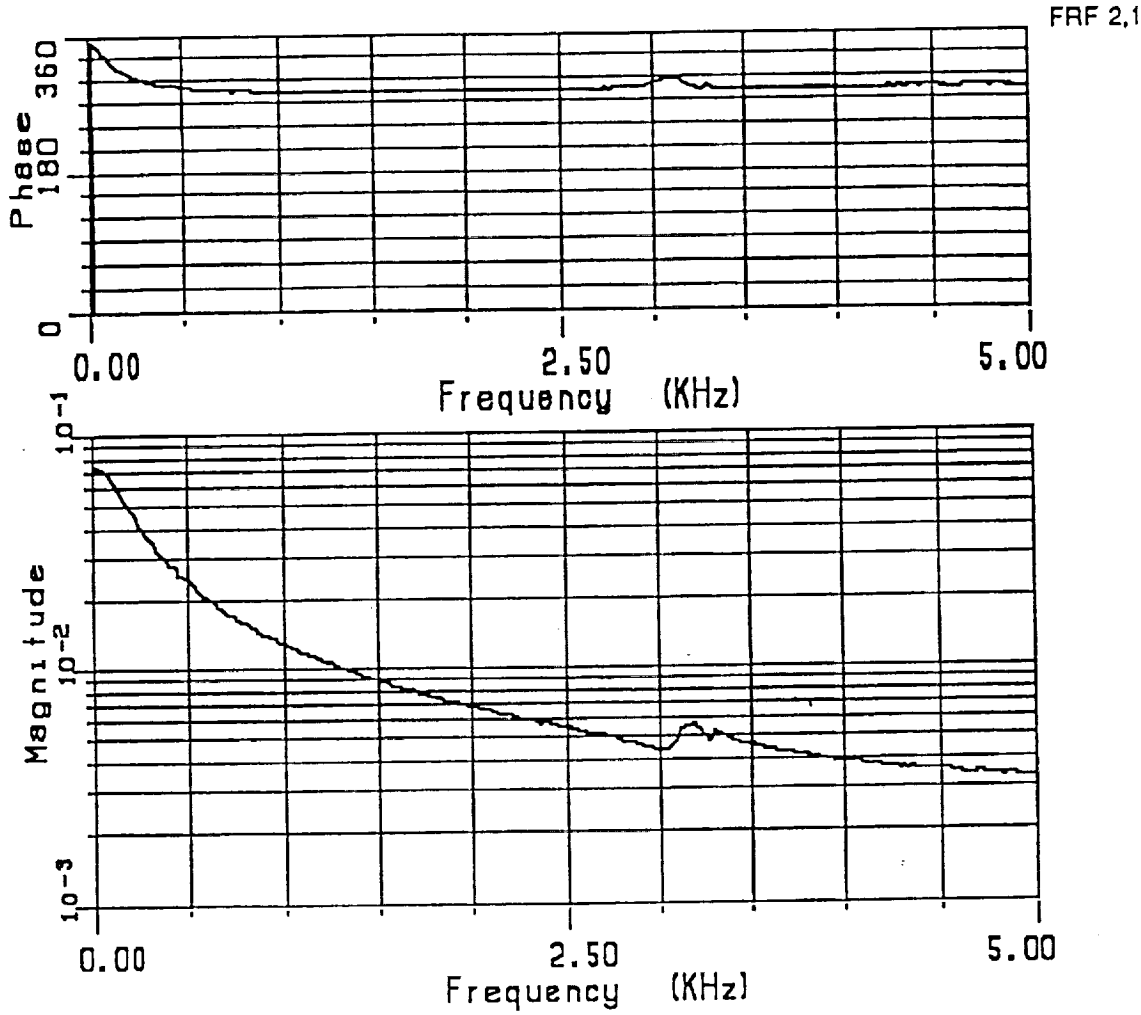

Figure 1.1 (d)

FRF30I/V

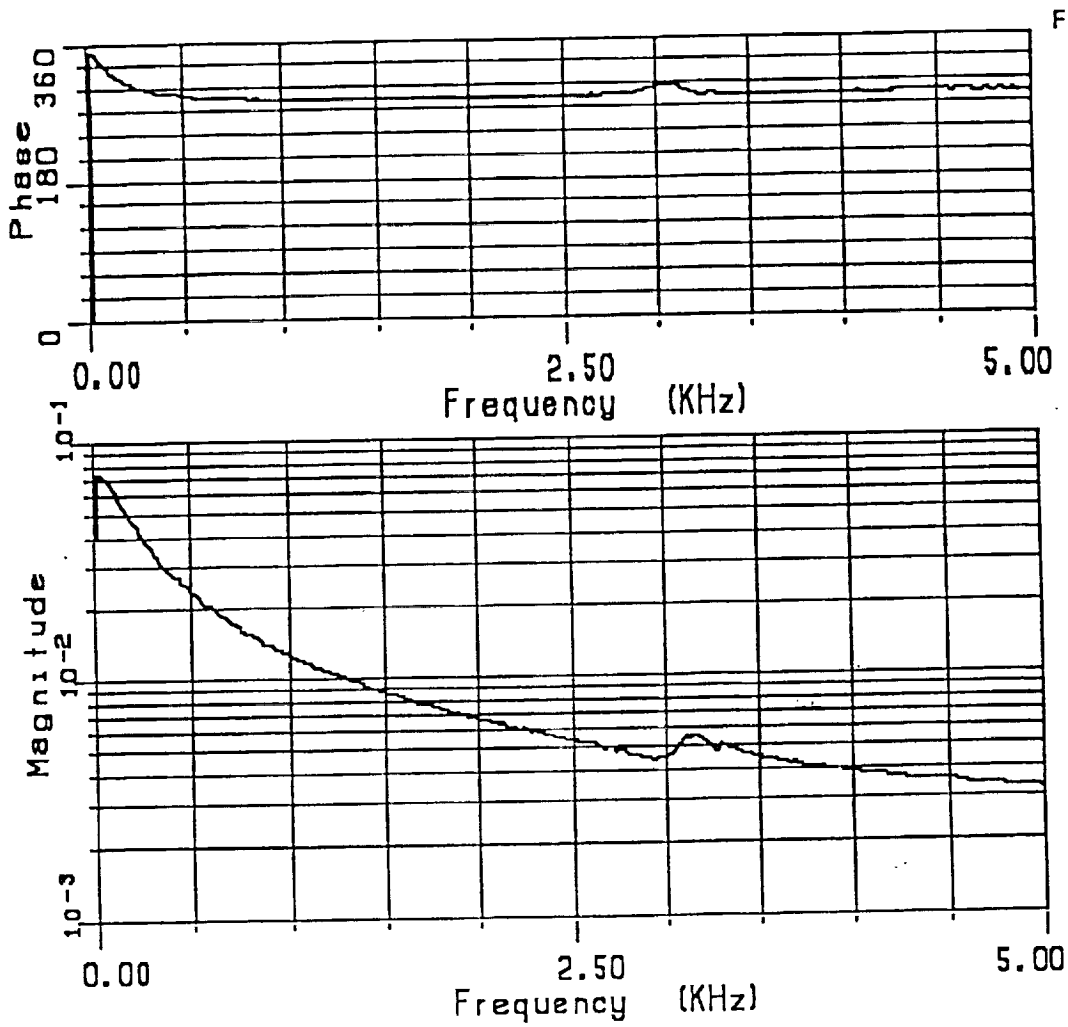

Figure 1.1 (e)

FRF60I/V

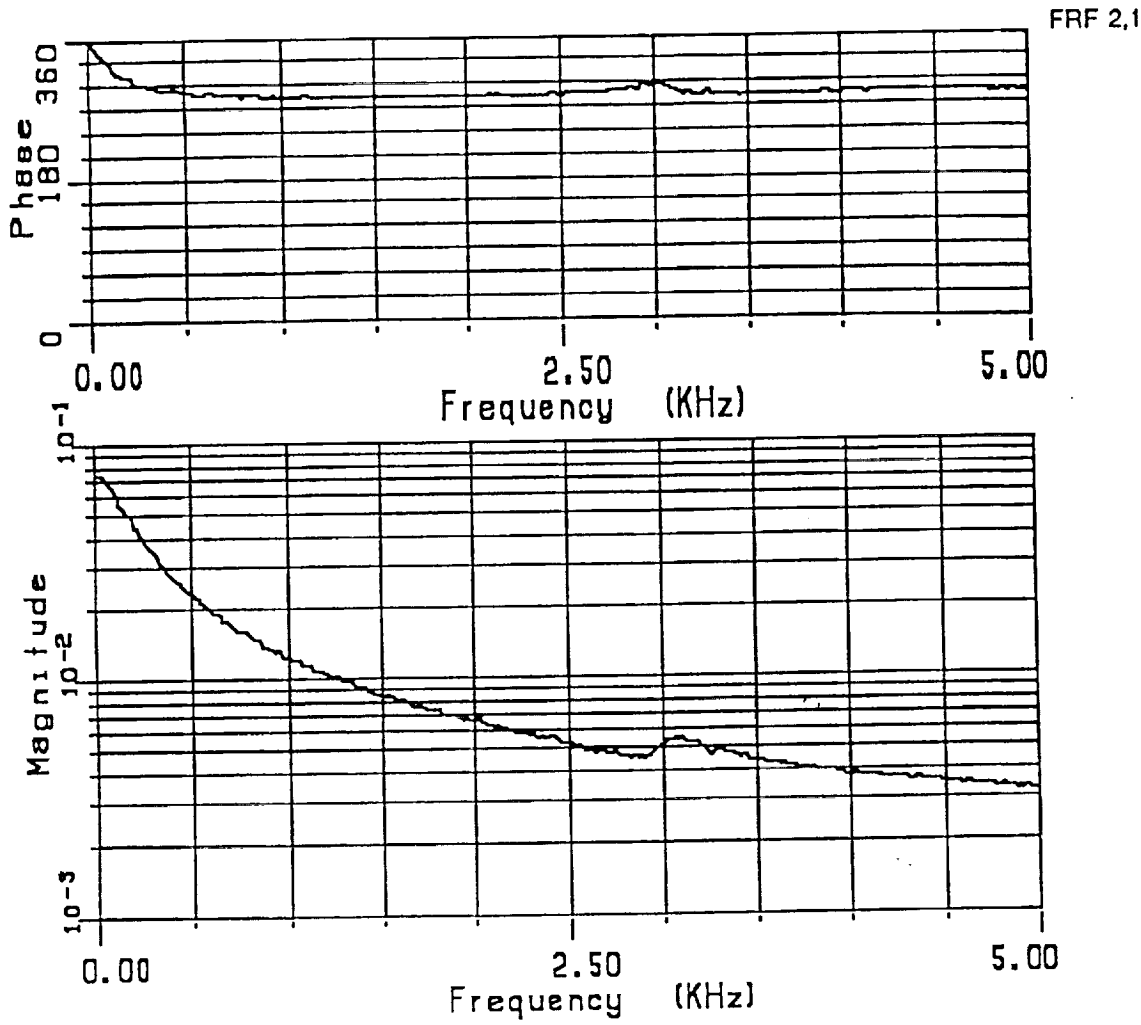

Figure 1.1 (f)

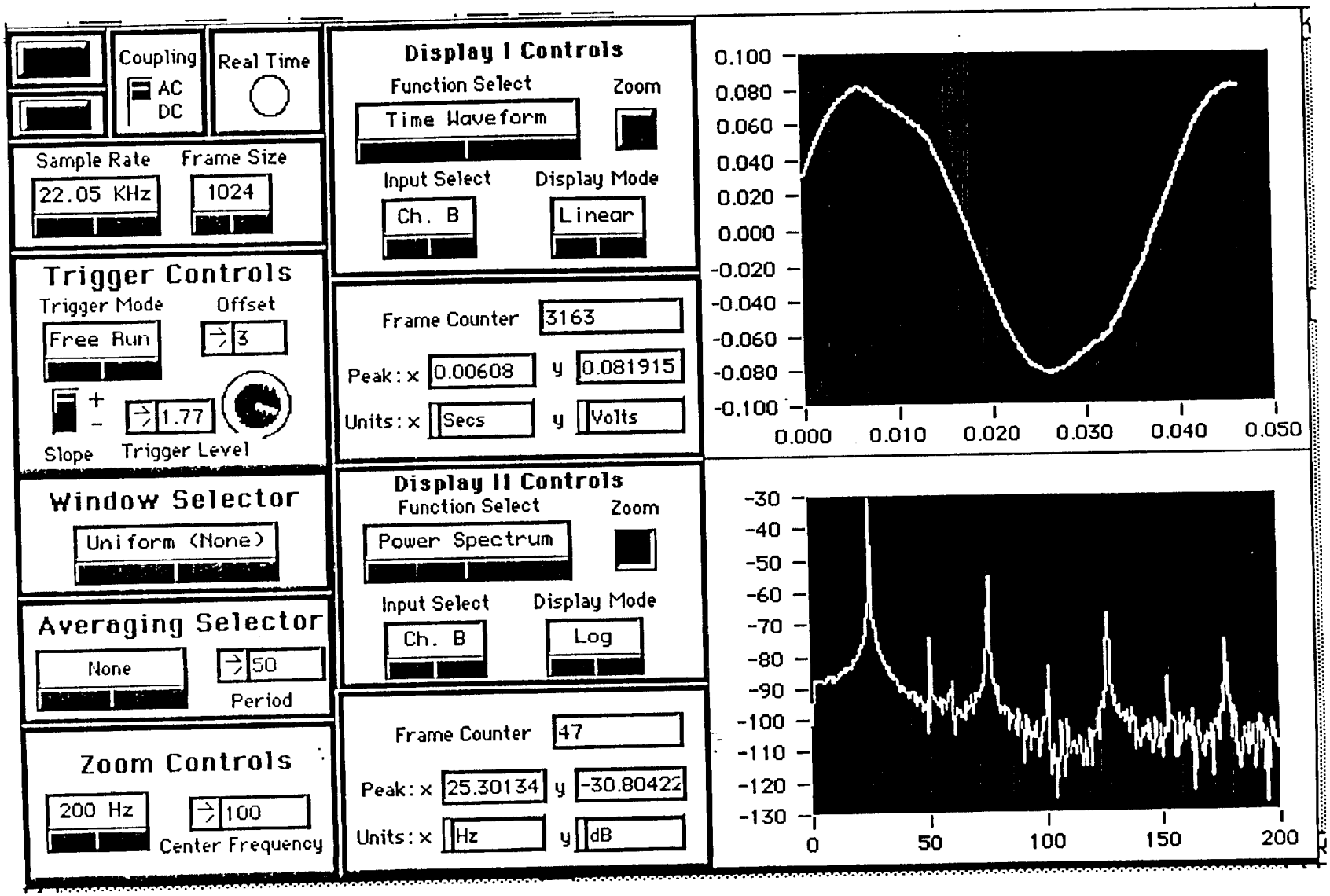

Figure 1.2 (a)

New Actuator With Mechanical Amplifier Test

Current Driven Mode: Voltage=0.27 V(pp), Current = 0.25 A (REM)

Displacement = 0.82 mils (pp)

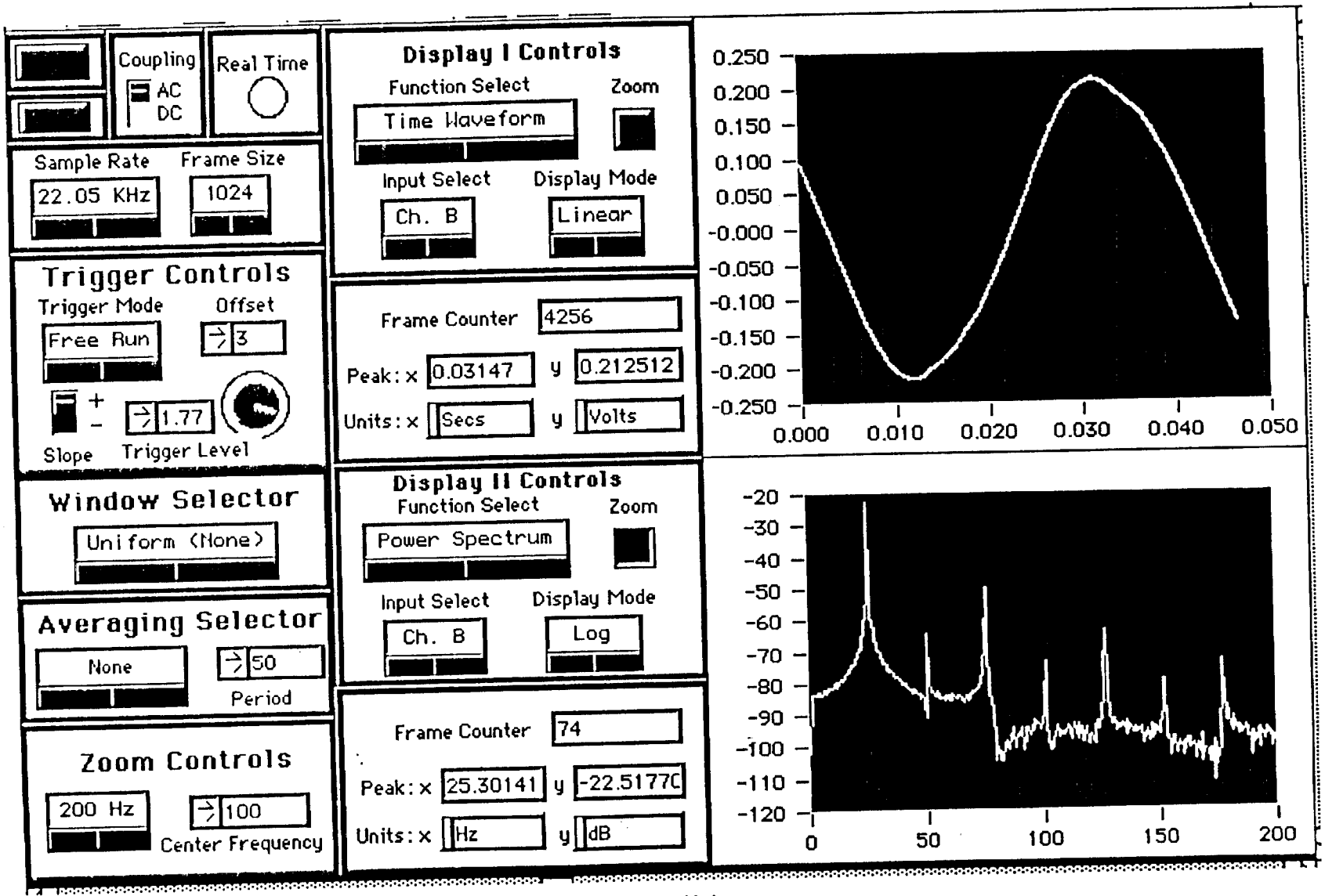

Figure 1.2 (b)

New Actuator With Mechanical Amplifier Test

Current Driven Mode: Voltage=0.51 V(pp), Current = 0.5 A (REM)

Displacement = 2.2 mils (pp)

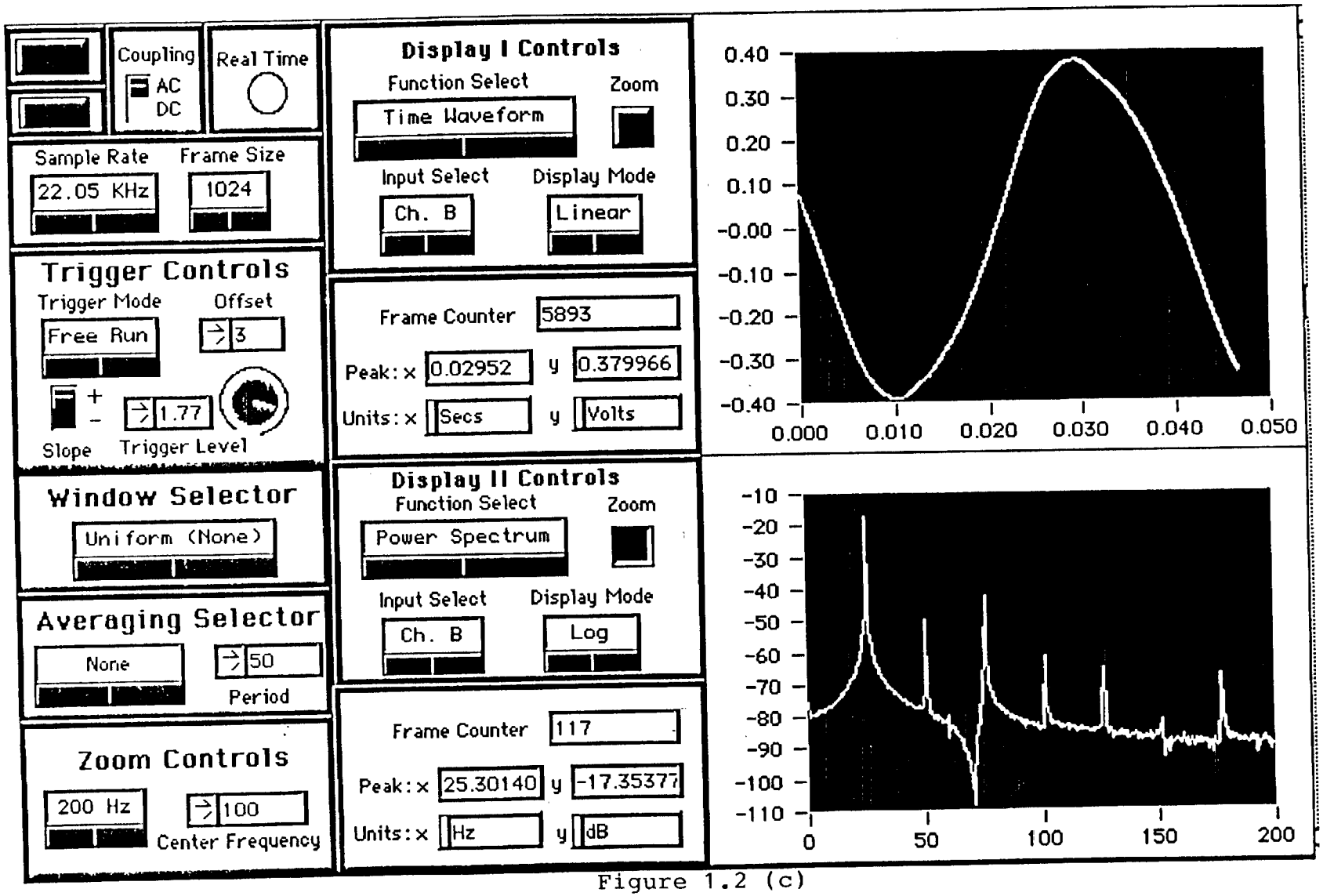

Figure 1.2 (c)

New Actuator With Mechanical Amplifier Test

Current Driven Mode: Voltage=0.76 V(pp), Current = 0.75 A (REM)

Displacement = 4 mils (pp)

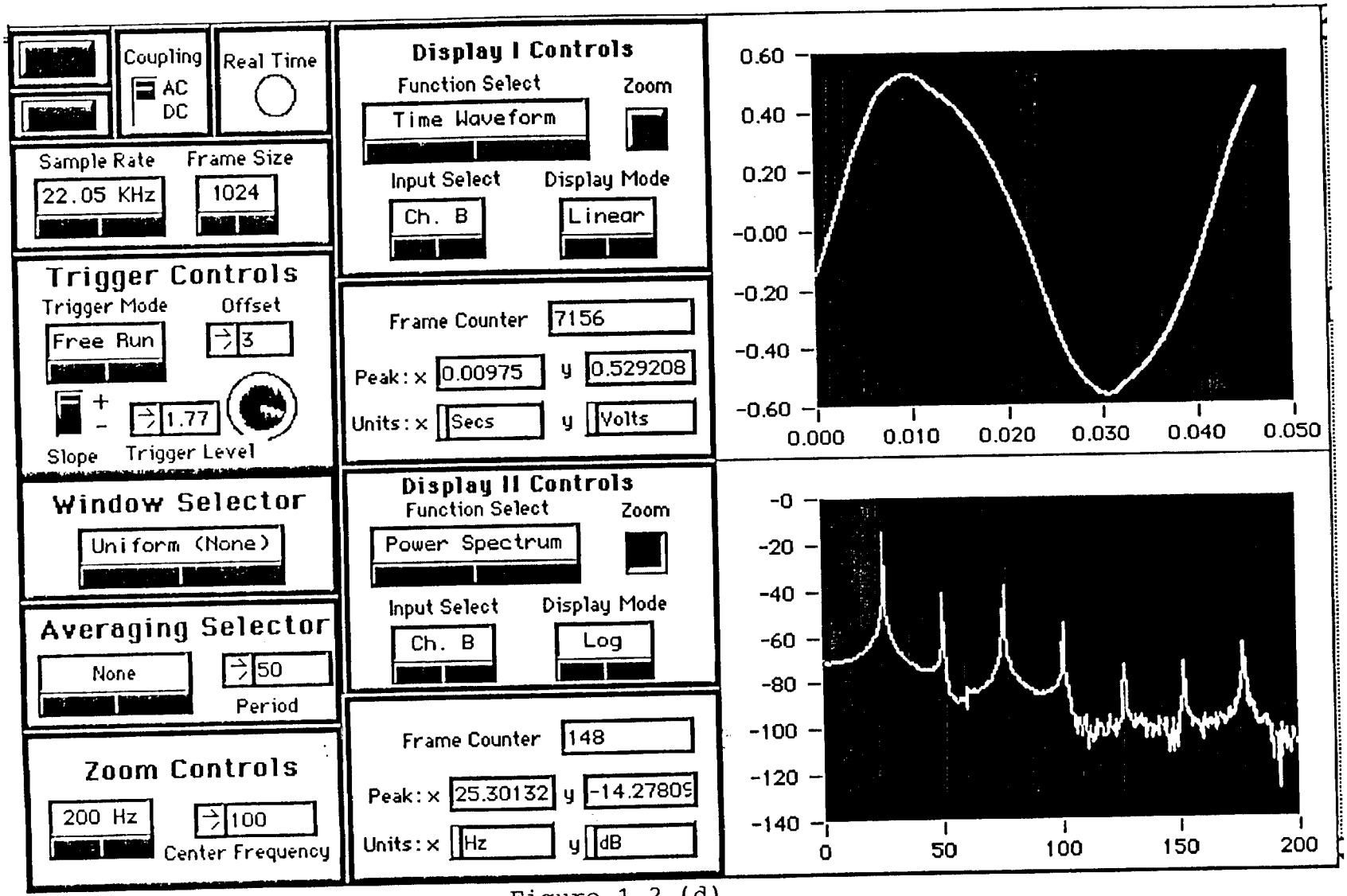

Figure 1.2 (d)

New Actuator With Mechanical Amplifier Test

Current Driven Mode: Voltage=1.0 V(pp), Current = 1.0 A (REM)

Displacement = 5.8 mils (pp)

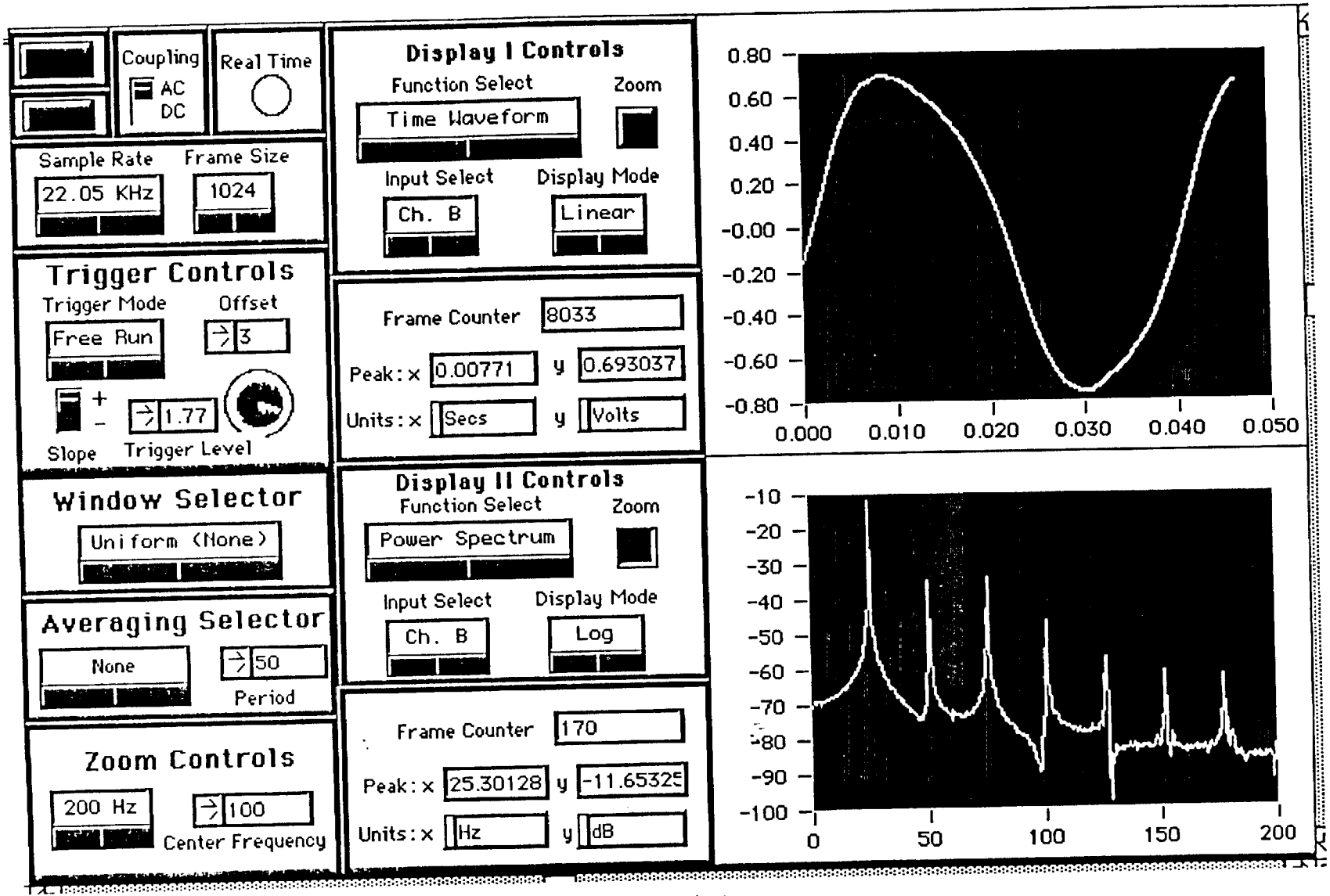

Figure 1.2 (e)

New Actuator With Mechanical Amplifier Test

Current Driven Mode: Voltage=1.25 V(pp), Current = 1.25 A (REM)

Displacement = 7.5 mils (pp)

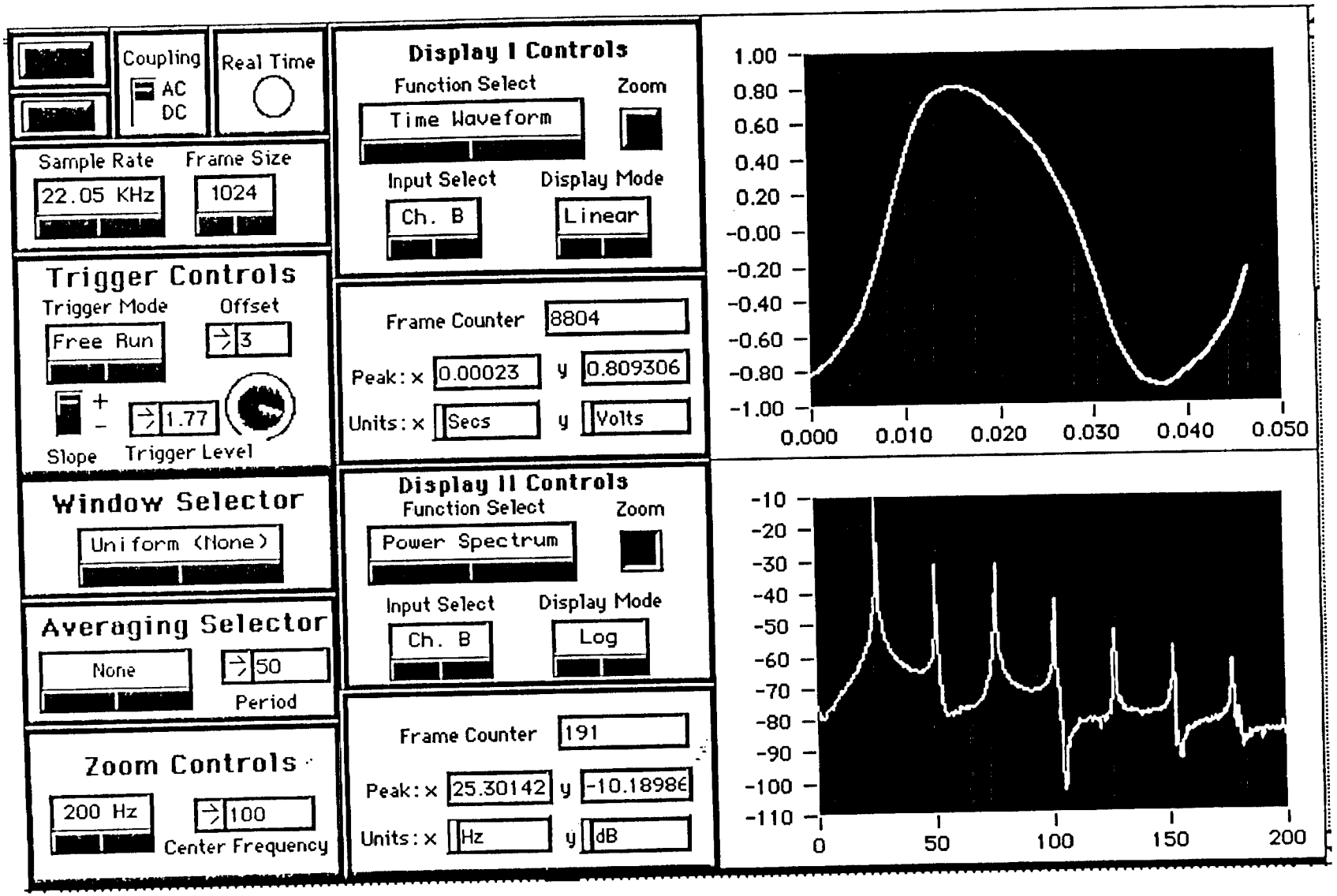

Figure 1.2 (f)

New Actuator With Mechanical Amplifier Test

Current Driven Mode: Voltage=1.49 V(pp), Current = 1.5A (REM)

Displacement = 8.5 mils (pp)

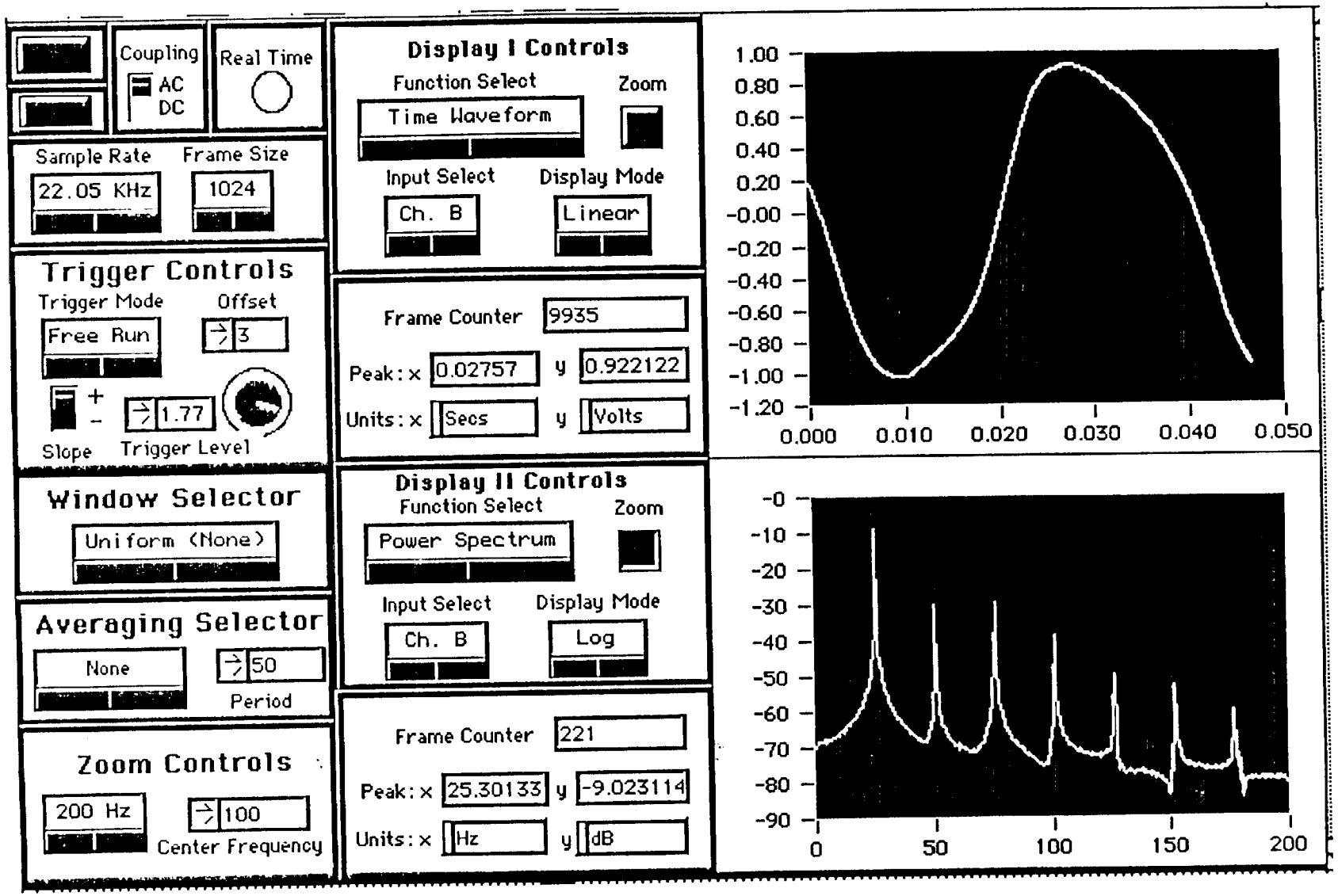

Figure 1.2 (g)

New Actuator With Mechanical Amplifier Test

Current Driven Mode: Voltage=1.73 V(pp), Current = 1.75 A (REM)

Displacement = 10 mils (pp)

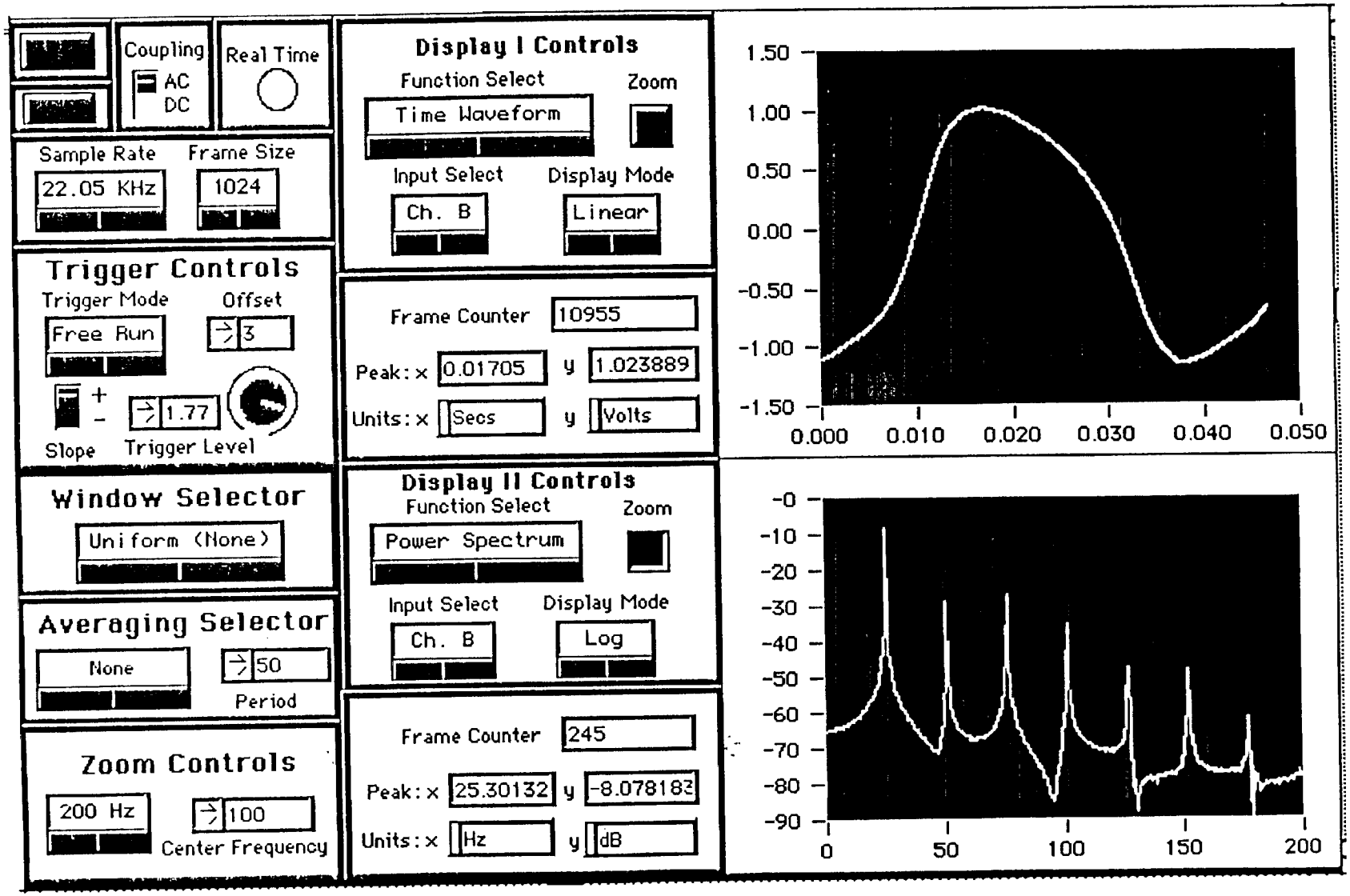

Figure 1.2 (h)

New Actuator With Mechanical Amplifier Test

Current Driven Mode: Voltage=1.97 V(pp), Current = 2.0 A (REM)

Displacement = 11.5 mils (pp)

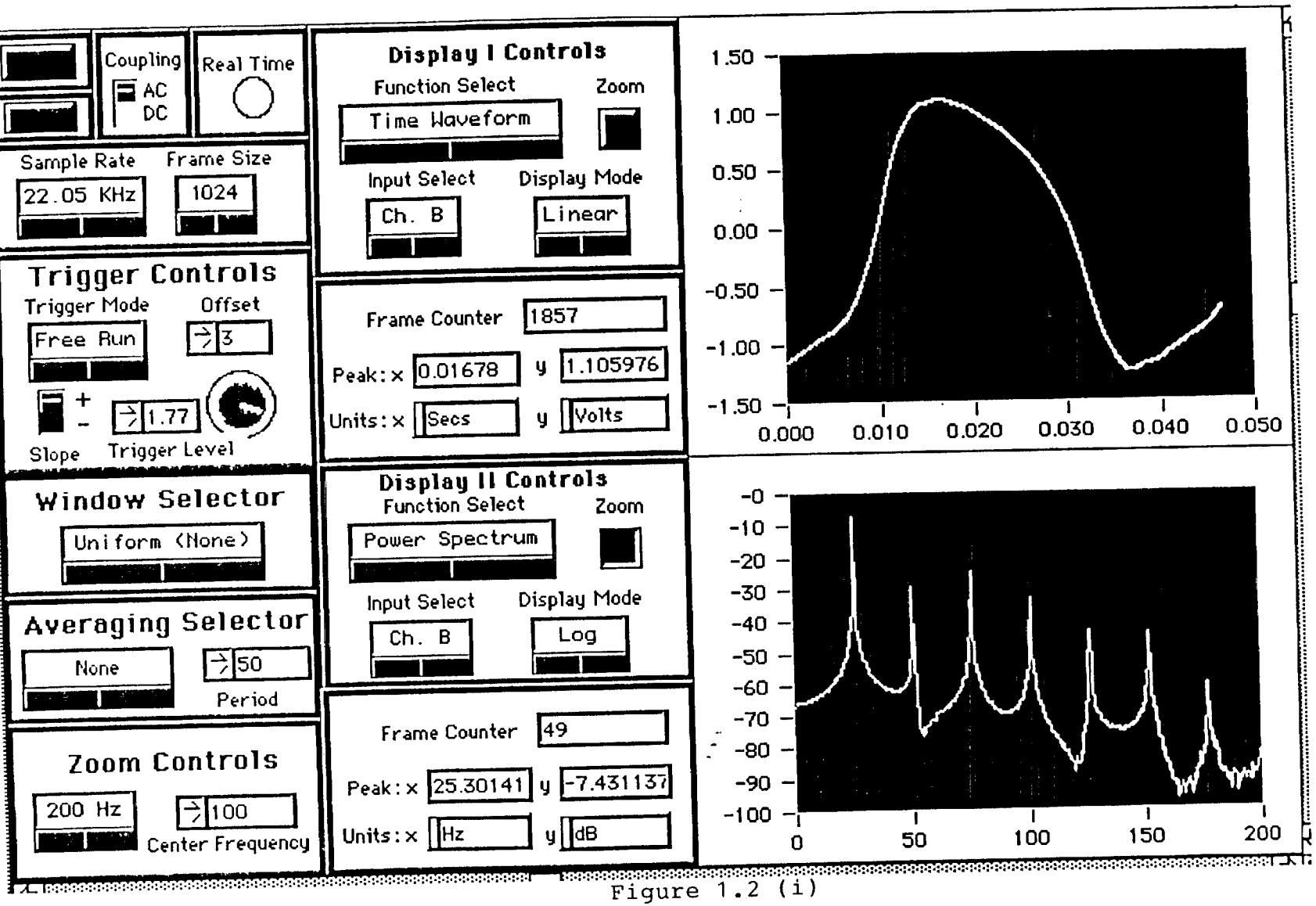

Figure 1.2 (i)

New Actuator With Mechanical Amplifier Test

Current Driven Mode: Voltage=2.21 V(pp), Current = 2.25 A (REM)

Displacement = 12 mils (pp)

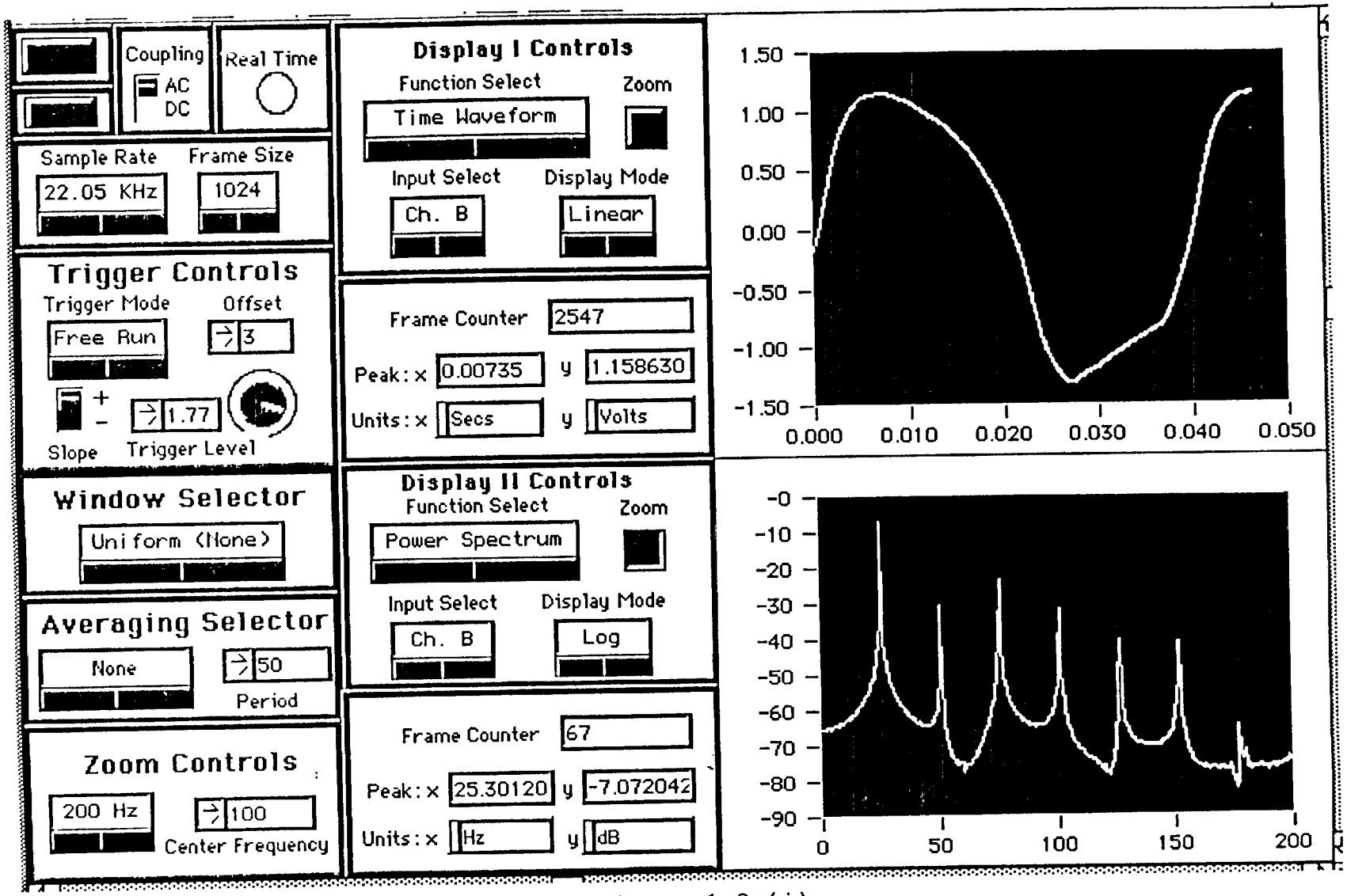

Figure 1.2 (j)

New Actuator With Mechanical Amplifier Test

Current Driven Mode: Voltage=2.45 V(pp), Current = 2.5 A (REM)

Displacement = 13 mils (pp)

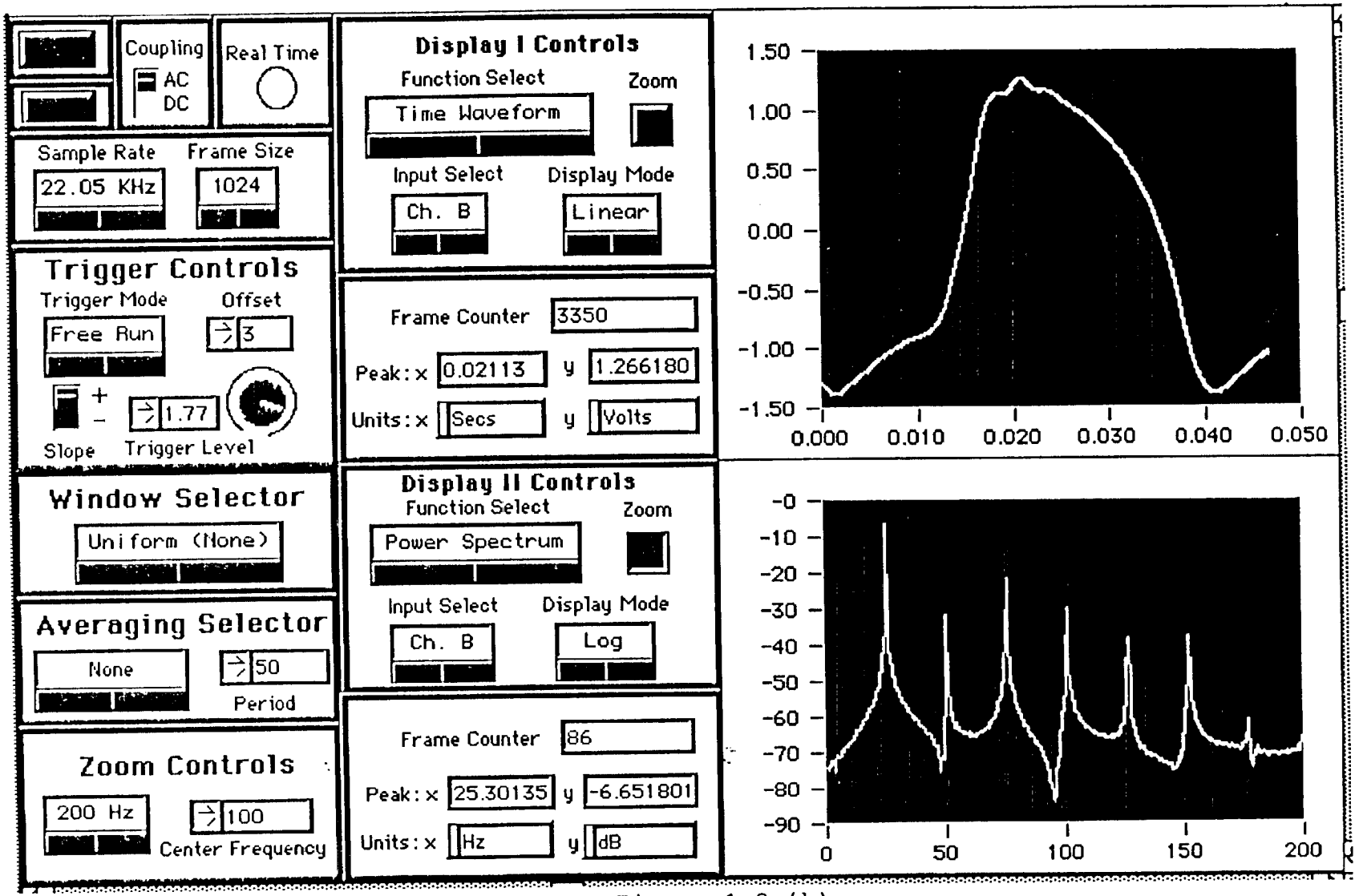

Figure 1.2 (k)

New Actuator With Mechanical Amplifier Test

Current Driven Mode: Voltage=2.69 V(pp), Current = 2.75 A (REM)

Displacement = 14 mils (pp)